

Zeeman Splitting in Mercury

Evan Berkowitz

Junior, MIT Department of Physics

(ΩDated: May 17, 2007)

We explore the phenomenon of weak-field Zeeman splitting, an effect which lifts the degeneracy in the quantum number m_j . We use a measurement of the splitting of the yellow doublet and green emission lines of mercury to determine e/m , the ratio of the elementary charge to the mass of the electron, to be $4.7 \pm 4 \cdot 10^{12}$ coulombs per kilogram, which is 7σ different from the accepted value.

1. INTRODUCTION

The familiar Coulomb potential description of hydrogen has a Hamiltonian

$$H_o = -\frac{\hbar^2}{2m} \nabla^2 - \frac{e^2}{r} \quad (1)$$

which gives eigenenergies

$$E_n = -\frac{\alpha^2 m c^2}{2} \frac{1}{n^2} \quad (2)$$

which only depend on n , where e is the elementary charge, m is the mass of the electron, c is the speed of light, and α is the fine structure constant. However, we know that a full description of an electron in the hydrogen atom requires four labels—the principal quantum number n , the orbital quantum number l , the magnetic quantum number m_l , and the spin quantum number m_s . Thus, we see that each energy level in a system only described by (1) is degenerate for all the allowed combinations of those additional quantum numbers.

However, when we observe atomic spectra, we observe many more transitions than just those between principal quantum numbers. These additional spectra lines must be explained in terms of the quantum numbers we have. The corrections are measured in strength by the order of α which appears in the energy. Two corrections, the relativistic correction and the spin-orbit coupling correction, are of order α^4 and are together termed the fine structure correction.

Their correction to Eq. (1) is given by

$$H_{\text{fine structure}} = H_{\text{relativistic}} + H_{\text{spin-orbit}} \quad (3)$$

where

$$H_{\text{relativistic}} = -\frac{p^4}{8m^3 c^2} \text{ and} \quad (4)$$

$$H_{\text{spin-orbit}} = \frac{e^2}{2m^2 c^2} \frac{1}{r^3} \vec{L} \cdot \vec{S}. \quad (5)$$

The relativistic correction arises by expanding the relativistic expression for kinetic energy in p and taking the first term of order higher than p^2 present in. The spin-orbit correction arises by considering the effect of the moving charged nucleus (from the electron's point of view) and the magnetic field which arises, adding a

term which correlates the electron's energy with its orbital quantum number l . The combined effect of the fine structure corrections is

$$E_{\text{fine structure}} = \frac{\alpha^4}{8} m c^2 \left(3 - \frac{4n}{j + \frac{1}{2}} \right). \quad (6)$$

This correction to the energy lifts the degeneracy of the states in l . Additionally, due to the spin-orbit coupling, \vec{L} and \vec{S} are no longer independently conserved, but instead are conserved as a sum $\vec{J} = \vec{L} + \vec{S}$. We trade quantum numbers m_l and m_s for j and m_j , where $\hbar^2 j(j+1)$ is the eigenvalue for J^2 and $\hbar m_j$ is the eigenvalue for J_z on a basis vector in the coupled basis, described by $|n \ l \ j \ m_j\rangle$. [1]

2. ZEEMAN SPLITTING

The fine structure corrections to the Coulomb Hamiltonian failed to lift the degeneracy in m_j . However, this does not imply that m_j is physically irrelevant to atomic spectra. One effect which depends on m_j is Zeeman splitting, which describes the splitting of spectral lines when the atom is placed into an external magnetic field. We add a term to the Hamiltonian

$$H_z = \frac{e}{2m} (L + 2S) \cdot \vec{B} = \frac{e}{2m} (J_z + S_z) B \quad (7)$$

where B is the strength of the magnetic field \vec{B} , and we drop the vector product by choosing the z -axis to be along the magnetic field. In the case of a weak field, we treat H_z as a perturbation to the Coulomb Hamiltonian corrected by the fine structure terms. Evaluating $\langle \vec{J} \cdot \vec{B} \rangle$ or equivalently $\langle J_z \rangle B$ is easy, as the basis vectors are eigenstates of J_z , and they contribute $\hbar m_j$. To evaluate $\langle \vec{S} \cdot \vec{B} \rangle$ or equivalently $\langle S_z \rangle B$ is more tricky. It is possible to use the Clebsch-Gordan coefficients to change back into the $|n \ l \ m_l \ m_s\rangle$ basis. Alternatively, we can visualize the problem for physical insight. The projection shown in Fig. 1 is justified because \vec{S} precesses quickly around \vec{J} , and thus the expected value of \vec{S} is simply its time average. Using the identity

$$\vec{S} \cdot \vec{J} = \frac{1}{2} (J^2 + S^2 - L^2) \quad (8)$$

we find

$$E_z = \mu_B B m_j \left[1 + \frac{j(j+1) - l(l+1) + s(s+1)}{2j(j+1)} \right]. \quad (9)$$

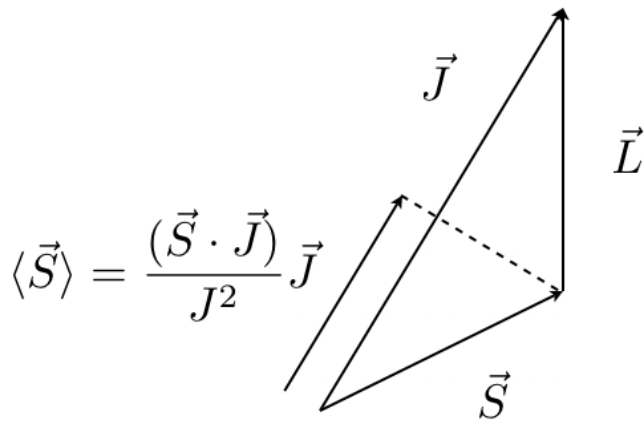


FIG. 1: A visualization of \vec{J} and the expectation of \vec{S}

where the Bohr magneton μ_B is defined as $\frac{e\hbar}{2m}$. We identify the term in the square bracket as g_j , the Landé g-factor.[2] The Landé g-factor is independent of m_j , so we see that the magnetic field splits each energy level into $2j + 1$ levels, since m_j runs from $-j$ to j in integer steps.

Defining wavenumber $\nu \equiv \frac{1}{\lambda}$, we can express the energy of a photon as $E = hc\nu$. Combining this relation with (9) we find that

$$\Delta\nu = \frac{\Delta E}{hc} = \frac{B}{4\pi c m} \frac{e}{\hbar} \Delta g_j \quad (10)$$

where Δg_j is the difference between the Landé g-factors of the two states involved in the transitions giving rise to those photons. Relation (10) provides a way for us to measure the ratio $\frac{e}{m}$, as all other values are known. We actually measure how the splitting changes as a function of magnetic field. Additionally, the splitting $\Delta\lambda$ is much smaller than the values of the two wavelengths, and thus we may approximate

$$\Delta\nu = \frac{1}{\lambda_1} - \frac{1}{\lambda_2} = \frac{\Delta\lambda}{\lambda^2} \quad (11)$$

Finally, we solve for $\frac{e}{m}$:

$$\frac{e}{m} = \frac{4\pi c}{\lambda^2 \Delta g_j} \frac{\Delta\lambda}{B} \quad (12)$$

We will measure the splitting $\Delta\lambda$ for many field strengths B and thus identify the final term $\frac{\Delta\lambda}{B}$ as the difference between the slopes of the peak splitting as a function of B .

In our experiment, we measure the green 5460.7\AA line of mercury and the yellow 5790.7\AA and 5769.6\AA yellow doublet. The green line arises from a transition between 3S_1 and 3P_2 . The yellow doublet arises from transitions between 3D_1 and 1P_1 as well as 3D_2 and 1P_1 respectively. The allowed transitions are given by the selection rule: $\Delta m_j = 0$ or ± 1 , and are shown in Fig. 2. Note that the green spectrum has 9 allowed transitions, resulting in 9 lines. In comparison, the yellow lines split

into three even though 7 and 9 transitions occur respectively, because the transitions give the same total energy difference. For the green lines, we calculate that Δg_j should be $\frac{1}{2}$ between two consecutive lines, and for the yellow lines, Δg_j should be 1 and $\frac{7}{6}$, respectively.

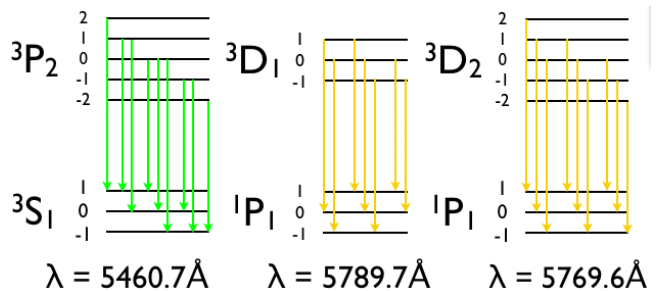


FIG. 2: Energy diagrams of the studied transitions. Note that the level splitting is greatly exaggerated compared to the transition energies.

3. EXPERIMENTAL APPARATUS

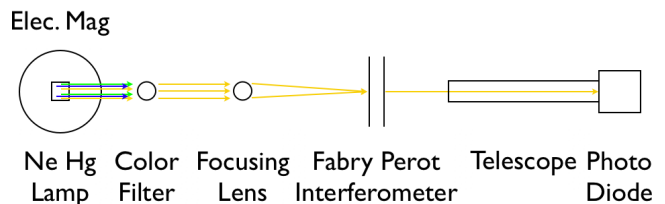


FIG. 3:

Figure 3 provides a schematic picture of our experimental setup. We had a neon-mercury lamp driven by a DC current of $\sim 20\text{mA}$ between the two faces of an Industrial Coils 37695 electromagnet.[3] It is this first part of the setup in which the physics occurs. The lamp was placed into a shield with a small circular hole, to prevent the lamp from being excessively bright and additionally to localize the source and minimize the interference effects from different parts of the lamp.

The emitted light was filtered by color and focused onto the Fabry-Perot interferometer. A Fabry-Perot interferometer is essentially two parallel glass plates which are highly reflective. The low transmission rate of light through the plates allows the light to reflect between the plates multiple times before emerging. The interference between the different paths the light can take causes only one particular wavelength to emerge axially centered, with other wavelengths forming a bullseye pattern around the optical axis. In particular, if a beam of light passes through the first plate at an angle θ and the plates are separated by a distance D , then the different paths that the light takes constructively interfere

will constructively interfere for a wavelength λ only if

$$2D \cos \theta = m\lambda \quad (13)$$

for some integer m . The left hand side describes the path difference the light takes, and the right hand side enforces the constructive interference requirement. The geometrical raytracing of the Fabry-Perot interferometer is shown in Fig. 4. One of the plates is mounted on

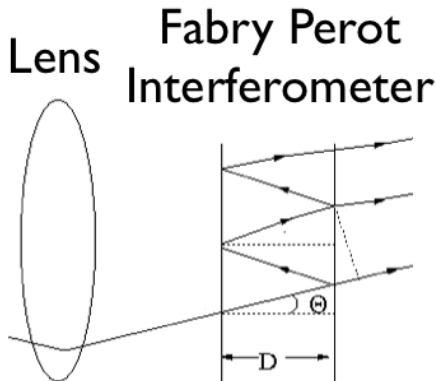


FIG. 4: A close-up of one beam of light passing through the Fabry-Perot interferometer. Taken from [3].

three micrometers, which we can adjust according to our choosing. The other plate is mounted on piezoelectric crystals, whose thicknesses change with the applied voltage. These crystals are controlled by a Burleigh RC-44 ramp generator, which sends slow sawtooth voltage ramps to those crystals, adjusting the plate separation and thus the wavelength which constructively interferes and is axially centered. By applying a large enough voltage ramp, we can sweep over a whole group of transitions. These optics allow for the naked-eye observation of Zeeman splitting.

Finally, the light was focused by a telescope onto a photomultiplier tube, which relayed the signal through a preamplifier and amplifier into an oscilloscope, which communicated with a computer and Agilent software over a COM port connection.

We recorded the magnetic field in terms of the current supplied, which ranged from 0 to 30 amperes, as this was the parameter which we could choose. In order to convert these settings into field strength for our measurement, we measured the magnetic field with a Walker MG-4D Hall Gaussmeter at currents between 0 and 30 amperes in steps of 5 amperes. As 30 amperes was the greatest current ever applied, a simple polynomial fit should suffice for interpolation to unmeasured currents. The magnetic calibration is shown in Fig. 5.

4. DATA AND ANALYSIS

Typical spectra are shown in Fig. 6. The analysis of green spectra was done by fitting 9 Lorentzians to the

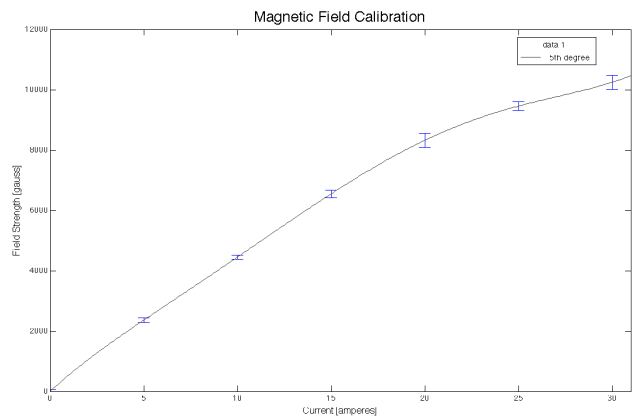


FIG. 5: The field calibration, allowing for easy exchange between current and field strength. The error bars are amplified 100 times for visibility. We use the fifth degree polynomial to interpolate to currents which were not measured.

spectra, though for lower currents fewer peaks are discernible and fewer Lorentzians were fit if it was apparent that some had simply merged and would not be found. After this fitting procedure, it was clear that the best-fit parameters were not sufficiently constrained. Thus, we only examined the tallest peaks, and the widest peaks, which were always easily identified by those fits.

The yellow spectra are more easily interpreted, and due to the relatively large amount of time it took for each Lorentzian fit and the , the peaks were found by smoothing the data and searching for local maxima, with errors assigned based upon the full width at half max of each respective peak.

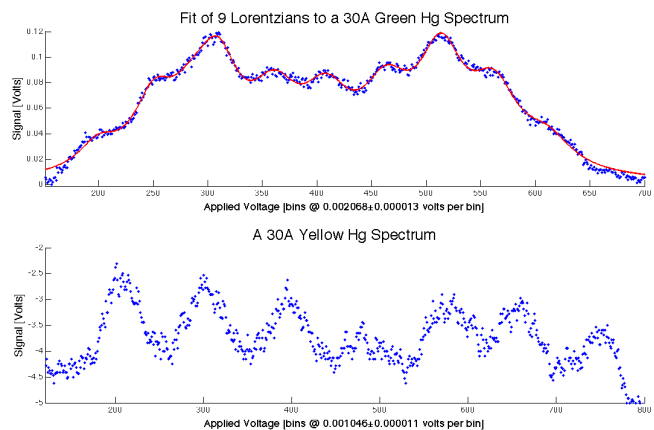


FIG. 6: A green spectrum with all 9 lines apparent and a yellow transition with 6 prominent peaks. The bump between the two sets of three in the yellow spectrum is interference from a separate order of lines.

When we visually observe the spectra, we can see the bullseye rings collapse one by one onto the center and dis-

appear. This indicates that mirrored plates are spreading apart, which in turn implies that longer wavelengths collapse after the shorter wavelengths. In order to remove the effect of differing positions of the spectra compared to one another, we subtract from all peak positions the average of those positions. This centers the spreading on 0, and allows us to align the centers of the spectra even though they do not correspond exactly in bins (voltage). The result of these operations for the yellow doublet is shown in Fig. 7. Each magnetic field strength was measured at least 3 times, and as many as 5. The errors shown are statistical.

Since the lines converge very near to zero applied current, it is fair to say that those points correspond to the wavelengths of the corresponding lines. As a result of our centering, the lower set of 3 lines arises from the 5770Å line and the upper set arises from the 5791Å line. We can use this information to calibrate our y -axis, as is done in Fig. 7. For green, the scale was not as clear-cut. To

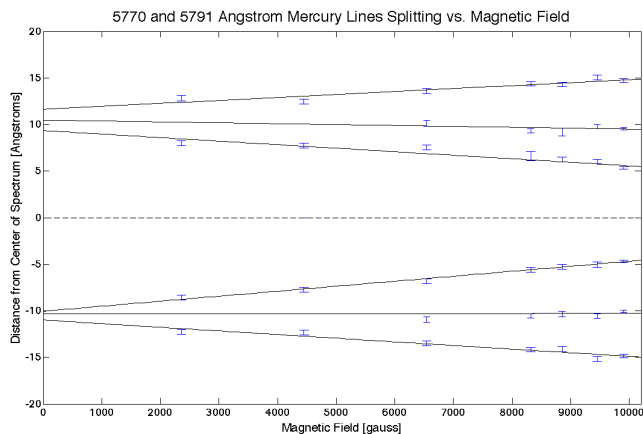


FIG. 7: The splitting of the yellow doublet as a function of applied field strength.

convert bin measurements (a difference in time) into a distance, we also examined the voltage ramp provided by the Burleigh controller and fit straight lines to them. Thus, a difference in bin measurement could be converted into a difference of voltage in a straightforward manner. Finally, we used a relation which follows from (13):

$$\delta\lambda = \lambda \frac{\lambda}{2D} \frac{\delta D}{\Delta D}, \quad (14)$$

where D is the plate separation, δD is the separation of the two transitions we wish to compare, and ΔD is the separation of one transition and the corresponding transition of another order. For a detailed explanation of this relation, see [3]. A geometric visualization of these variables is shown in Fig. 8. The plate separation corresponds to the chosen micrometer setting, with a known offset of $12212 \pm 15 \mu\text{m}$. Instead of measuring δD and ΔD in length, we measure equivalently in voltage applied by the Burleigh controller to the piezoelectric actuators. The green data is omitted for brevity.

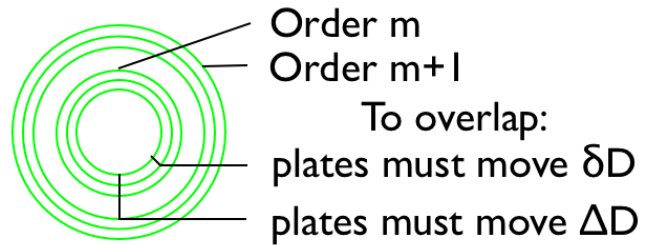


FIG. 8: A visual mnemonic of the difference between ΔD and δD .

In (12) we identified $\frac{\Delta\lambda}{\lambda}$ as the slope difference between two consecutive lines, shown in Fig. 7. Using these values to calculate e/m , we arrive at a best value of 4.7 ± 0.4 coulombs per kilogram, which disagrees significantly with the NIST value of 1.758 coulombs per kilogram by 7.5σ . Unfortunately, after an extensive review of our data, procedure and analysis, and a discussion with peers, we are unable to justify a multiplicative factor, leaving our of the correct order, but unreasonably high and in disagreement with a well established value.

5. ERROR

Our quantity, which does not agree well with the accepted value, still contains an uncertainty of 10%. This 10% is solely from the statistical error which propagated through our calculation from the various measurements we made of each magnetic field strength. Additionally, we must estimate the systematic errors on our values. Fortunately, few effects effect the spreading of the peaks in a particular spectrum, as most effects change the amplitude of the signal.

First, it is extremely difficult to focus the telescope such that the peaks are as well defined as one sees by peering through the interferometer. This causes uncertainty in the peak locations, already accounted for in the 10% statistical error. Additionally, order to apply the pertinent equations, the reflective plates should be parallel. Any deviation from parallel would upset the interference and cause a shift of peaks, possibly depending on the wavelength of the peak. However, by examining the “breathing” of the spectrum—the growing and shrinking of the bullseye pattern—a shift from the optical axis—with the naked eye we were able to effectively remove this concern, the breathing seen at a typical distance for the telescope’s lens was less than 1% of the total radius for perturbations of the viewpoint on the order of the radius of the telescope’s lens.

Errors unaccounted for include the mechanical uncertainty inherent in the micrometers and the local field fluctuations. The distance between the plates was typically on the order of 1mm and the micrometer settings had mechanical leeway of the order of $25\mu\text{m}$ in either direction, making this error on the order of 2.5%. This error

could be removed via a systematic method of setting the micrometers and ensuring nothing disturbs the interferometer.

While measuring the magnetic field we learned that the

field could fluctuate by about 30 gauss over a distance on the order of the size of the mercury lamp. This error is less than 1%, as all data at nonzero current was taken at a field strength of the order of 1000 gauss.

-
- [1] H. Liu, *X.5 The Fine Structure of Hydrogen* (2007).
 - [2] H. Liu, *X.6 The Zeeman Effect* (2007).
 - [3] S. Sewell, *The zeeman effect and hyperfine structure in mercury*, <http://web.mit.edu/8.13/www/JLExperiments/JLExp06.pdf> (2007).